Available online at www.sciencedirect.com

ScienceDirect

Ceramics International 39 (2013) 8901–8909

CERAMICS INTERNATIONAL

www.elsevier.com/locate/ceramint

Origin of anomalous octahedral distortions and collapse of magnetic ordering in $Nd_{1-x}Sr_xFeO_3$ ($0 \leq x \leq 0.5$)

I. Ahmad[a,b], M.J. Akhtar[a,*], M. Siddique[a], M. Iqbal[a], M.M. Hasan[b]

[a]*Physics Division, PINSTECH, P.O. Nilore, Islamabad, Pakistan*
[b]*Department of Metallurgy and Materials Engineering, PIEAS, Islamabad 45650, Pakistan*

Received 25 January 2013; received in revised form 23 April 2013; accepted 24 April 2013
Available online 9 May 2013

Abstract

The effects of strontium doping on the structural properties and magnetic ordering of $Nd_{1-x}Sr_xFeO_3$ orthoferrite system have been studied by employing macroscopic and microscopic structural techniques like X-ray diffraction, scanning electron microscopy and ^{57}Fe Mössbauer spectroscopy. X-ray diffraction confirmed that single phase materials have been synthesized. It has been observed that orthorhombic distortion, density and porosity have decreased; whereas, grain size, tolerance factor and symmetry have increased with increase in the strontium concentration. Mössbauer results showed an increase in the Fe^{4+}/Fe^{3+} ratio, sagging and local octahedral distortions while decrease in the magnetic ordering with increase in the strontium content. The origin behind anomalous octahedral distortions in this system has been attributed to the decrease in the oxidation state and mismatch in the ionic radii of A-site cations and increase in the concentration of Fe^{4+}, due to Sr^{2+} doping at Nd^{3+} sites. The collapse of magnetic ordering has been ascribed to the weakening of super-exchange interactions, dilution of strong long range magnetic sub-lattice of high spin Fe^{3+} (five unpaired electrons) by relatively lower spin of high spin Fe^{4+} (four unpaired electrons) and increase in the spin–spin relaxation frequency.

Keywords: $Nd_{1-x}Sr_xFeO_3$; Mössbauer; Octahedral distortions; Magnetic ordering; Super-exchange

1. Introduction

Perovskite type metal oxides are widely studied both theoretically and experimentally due to very broad range of electrical properties from insulators to superconductors [1–5], metal to insulator transitions [6], magnetic properties [7], magneto-resistive properties [8,9], electrochemical and catalytic properties [10]. These properties make these materials important for numerous hi-tech applications such as solid oxide fuels cells [11–13], gas sensors, catalysis [14,15], spin valves, magnetic field sensors [16], environmental monitoring applications [17] and spintronic devices [18]. The chemical doping is a valuable tool for improving different physical and chemical properties of materials. Doping can bring about changes in conductivity, oxidation states, bond lengths, bond angles, lattice distortions, lattice parameters, phase transitions and controls the properties of any material. In the case of $AFeO_3$ orthoferrites, (where A = rear earth cation, e.g. La, Nd, Y, etc.), doping at A-site with alkaline earth metals (such as Ca or Sr) increases the electronic and ionic conductivities due to hole formation or formation of oxygen vacancies depending upon the synthesis conditions. In the past few decades much attention has been given to doped and undoped $NdFeO_3$ orthoferrites and the effects of doping on the structural, electrical and magnetic properties have been investigated [19,20].

The crystal structure of $NdFeO_3$ is orthorombically distorted derivative of cubic perovskites with *Pbnm* symmetry. The crystallographic unit cell can be visualized as three dimensional tilted, slightly deformed and corner sharing FeO_6 octahedra, while the A-site cations (Nd^{+3}) are dodecahedrally coordinated by 12 O^{-2} ions and fit in the cavities between eight FeO_6 octahedra, as shown in Fig. 1. In case of FeO_6 octahedra, the Fe–O bond distances of all the six oxygen atoms are not equal, the oxygen atoms in the orthoferrite compounds occupy two distinct crystallographic positions, namely O1

*Corresponding author. Tel.: +92 51 9248801; fax: +92 51 9248808.
E-mail addresses: javedakhtar6@gmail.com, javed06@yahoo.com (M.J. Akhtar).

0272-8842/$ - see front matter © 2013 Elsevier Ltd and Techna Group S.r.l. All rights reserved.
http://dx.doi.org/10.1016/j.ceramint.2013.04.084

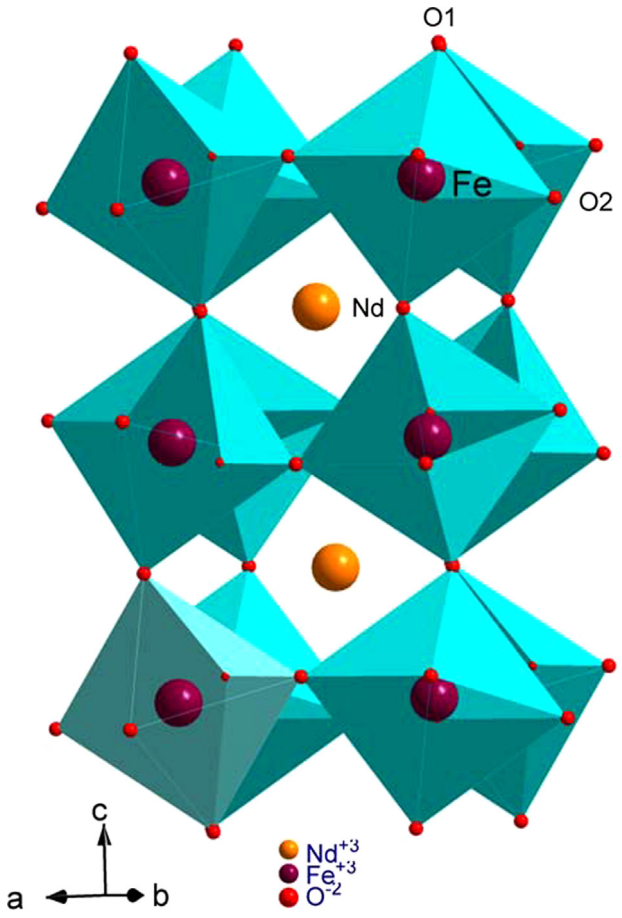

Fig. 1. Distorted perovskite structure of $NdFeO_3$.

which is along [001] direction forming two apices and O2 perpendicular to [001] direction forming remaining four apices in the plane of the octahedra. All Fe–O1–Fe and Fe–O2–Fe bond angles are less than 180° in these compounds, and each Fe ion is coupled by superexchange interaction with six nearest Fe ions, resulting in antiferromagnetic ordering while weak ferromagnetism is observed due to canting of spins. The Neel temperature of $NdFeO_3$ is 760 K which decreases with increase in the strontium content [21–23]. Brinks et. al. [24] have observed a decrease in the Neel temperature of $Pr_{1-x}Sr_xFeO_3$, similar findings were also observed by Kharton et. al. [25] in different orthoferrites.

The ground state electronic structure of perovskite based orthoferrites is controlled by the interaction between on-site coulomb strength (U), the charge transfer energy (Δ), the hybridization strength between metal 3d and oxygen 2p states (t) and crystal field splitting of the FeO_6 octahedra. The interplay between these parameters shows extremely wide-ranging properties [26].

The physical properties of a material strongly depend upon its structure. Usually, macroscopic characterization techniques such as X-ray diffraction (XRD) or Neutron diffraction are employed for the determination of structural parameters. However, both techniques determine the average crystal structure of a material and do not provide much information about the local structure, which is sometimes more important for understanding the correlation between properties and structure of the material.

The scanning electron microscopy (SEM) is a useful technique for the microstructural investigations of materials. This technique provides information about grain or particle size, grain morphology, grain size distribution, grains connectivity, grain boundaries, segregation, presence of cracks in the material, welding of dissimilar materials, effects of temperature and dopants on grain size and porosity present in the materials [27–28].

For the determination of local structural environment of materials, Mössbauer spectroscopy is a very helpful microscopic technique. This technique is capable of exploiting structural, chemical, electronic and magnetic properties of the material via hyperfine interactions. These hyperfine interactions give rise to Mössbauer parameters such as isomer shift, quadrupole splitting, line width and magnetic Zeeman splitting, which are very sensitive to crystal chemistry, atomic surrounding, spin state, oxidation state of an atom and can be used to investigate subtle changes due to chemical doping or because of any other external perturbation such as temperature, pressure or magnetic field [29–32]. Since, the electrical conduction in orthoferrites is due to 3d electrons of transition metal ions which strongly depend on the oxidation as well as spin state of the metal ions. Therefore, the information collected by ^{57}Fe Mössbauer spectroscopy is extremely useful in understanding the electrical conduction in these materials. This technique can determine the minute changes in local atomic and electronic structure around the probing nuclei. The objective of present study is to investigate how hyperfine interactions evolve in $Nd_{1-x}Sr_xFeO_3$ system due to strontium doping.

2. Experimental

Polycrystalline $Nd_{1-x}Sr_xFeO_3$, (where x=0, 0.1, 0.2, 0.3, 0.4 and 0.5), samples were synthesized in air by the conventional solid state reaction method, using high purity (99.99%) Nd_2O_3, $SrCO_3$ and Fe_2O_3 obtained from Sigma-Aldrich. To get a homogenous mixture, stoichiometric amounts of the starting materials were mixed in high purity acetone followed by grinding. The mixtures of oxides and carbonate were heated at 1000 °C, 1100 °C and 1200 °C for 16 h at each temperature with intermediate grinding. After this heat treatment, circular pellets of 10 mm diameter and ~1.5 mm thicknesses were fabricated under a pressure of 3 t/in.^{2}. These pellets were finally sintered at 1300 °C for 16 h. Heating rate was maintained at 5 °C/min during sintering at each temperature, while all samples were cooled in closed off furnace. The phase purity of the sintered pellets was confirmed by X-ray diffraction (XRD) using Cu K_α radiation (1.5418 Å). The room temperature XRD data were collected for $20° \leq 2\theta \leq 70°$ with 0.02° scanning step size and 3 s per step counting time. In order to calculate the lattice parameters least square fitting procedure was employed. Densities of these sintered pallets were measured using pycnometer. For SEM analysis each sintered

pallet was fractured perpendicular to the circular plane and analyses of these fractured surfaces were carried out by using scanning electron microscope (Leo 440i). Fe^{57} Mössbauer spectra were taken at room temperature in the transmission mode using Co^{57} in Rh matrix as a source of γ-rays. For calibration of the Mössbauer spectrometer, a thin α-Fe foil was used. MOS-90 computer program was used to analyze the Mössbauer data; analysis was performed assuming that all peaks were Lorentzian in shape.

3. Results and discussion:

Fig. 2 shows the XRD patterns of freshly synthesized samples of $Nd_{1-x}Sr_xFeO_3$ (where $x=0$–0.5) collected at room temperature. The XRD spectra were indexed on the basis of orthorhombic perovskite structure having space group *Pbnm*, on the basis of PCPDF Card no. 82-2421. The lattice parameters, *a*, *b* and *c*, calculated from these data are shown in Table 1; which are consistent with the earlier reported work [19,20,25,33,34]. From these results we note that some peaks between 30–35° and 55–60° in the XRD patterns, which are visible in un-doped $NdFeO_3$ sample, gradually merge into single peaks with increase in the strontium content indicating

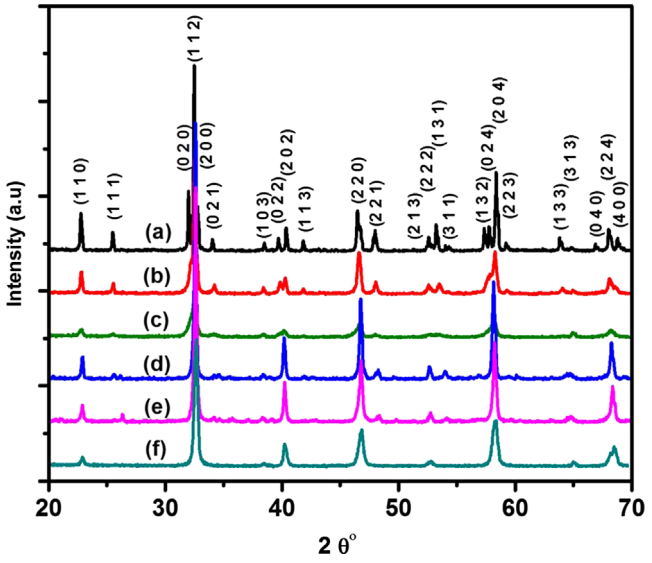

Fig. 2. XRD patterns of (a) $NdFeO_3$ (b) $Nd_{0.9}Sr_{0.1}FeO_3$ (c) $Nd_{0.8}Sr_{0.2}FeO_3$ (d) $Nd_{0.7}Sr_{0.3}FeO_3$ (e) $Nd_{0.6}Sr_{0.4}FeO_3$ and (f) $Nd_{0.5}Sr_{0.5}FeO_3$ collected at room temperature.

Table 1
Phase symmetry, cell parameters (*a*, *b* and *c*), and cell volume of $Nd_{1-x}Sr_xFeO_3$.

Sample	Phase symmetry	*a* (Å)	*b* (Å)	*c* (Å)	Cell volume (Å^3)
$NdFeO_3$	Orthorhombic	5.459	5.593	7.761	236.97
$Nd_{0.9}Sr_{0.1}FeO_3$	Orthorhombic	5.466	5.568	7.765	236.33
$Nd_{0.8}Sr_{0.2}FeO_3$	Orthorhombic	5.464	5.562	7.763	235.92
$Nd_{0.7}Sr_{0.3}FeO_3$	Orthorhombic	5.470	5.533	7.778	235.43
$Nd_{0.6}Sr_{0.4}FeO_3$	Orthorhombic	5.467	5.519	7.766	234.11
$Nd_{0.5}Sr_{0.5}FeO_3$	Orthorhombic	5.463	5.499	7.762	233.25

an increase in the symmetry; which infers a shift from orthorhombic to more symmetric tetragonal or cubic phase. By comparing the changes in lattice parameters, it has been observed that change in the *b* parameter is more pronounced than that of *a* and *c* parameters. The cell volume is maximum for $NdFeO_3$ which decreases gradually with increase in the strontium concentration. The reason for this decrease is that when trivalent Nd ions are replaced by divalent Sr ions, then in order to maintain the charge neutrality some of Fe^{3+} ions are converted into Fe^{4+} ions, causing a reduction in the Fe–O bond lengths. Consequently, the size of the octahedron decreases which results in a reduction of the unit cell volume and the system changes from orthorhombic to more symmetric tetragonal or cubic phase. This trend has also been confirmed by the Goldsmith tolerance factor (*t*), calculated from ionic sizes given by Shannon [35], and orthorhombic distortion parameter (*D*) as reported in Table 2. The value of Goldsmith tolerance factor increases with increase in the strontium concentration. The Goldsmith tolerance factor has been calculated by using the following formula:

$$t = \frac{d_{A-O}}{\sqrt{2}\,(d_{B-O})} = \frac{r_A + r_O}{\sqrt{2}(r_B + r_O)} \quad (1)$$

The orthorhombic distortion parameter (*D*), which measures the deviation of unit cell from ideal cubic structure, has been obtained by the following equation:

$$D = \frac{1}{3}\sum_{i=1}^{3}\left|\frac{\alpha_i - \overline{\alpha}}{\overline{\alpha}}\right| \times 100 \quad (2)$$

Here, $\alpha_1 = a$, $\alpha_2 = b$, $\alpha_3 = c/\sqrt{2}$ and $\overline{\alpha} = (abc/\sqrt{2})^{1/3}$ [36]. The observed value of orthorhombic distortion is maximum for undoped $NdFeO_3$, which reduces gradually with increase in the strontium concentration.

The density of a material is a very important parameter for the determination of electrical and thermal properties and the value bulk density must be above 90% of the theoretical density [19]. In this study, bulk density of $Nd_{1-x}Sr_xFeO_3$ was measured by using a pycnometer, while theoretical density was calculated by employing the following formula:

$$d_{th} = ZM/NV \text{ g/cm}^3 \quad (3)$$

In Eq. (3), *Z* is the number of formula units in one unit cell and its value is 4 for $GdFeO_3$ type structures. *M* is the atomic

Table 2
Calculations of Goldsmith tolerance factor, orthorhombic distortion parameter, XRD density, bulk density and calculated porosity of $Nd_{1-x}Sr_xFeO_3$ samples.

Sample	Goldsmith tolerance factor (*t*)	Orthorhombic distortion parameter (*D*)	XRD density d_{th} (g cm^{-3})	Bulk density *d* (g cm^{-3})	Calculated porosity *P* (%)
$NdFeO_3$	0.9232	0.9616	6.953	6.756	2.833
$Nd_{0.9}Sr_{0.1}FeO_3$	0.9291	0.7219	6.813	6.656	2.304
$Nd_{0.8}Sr_{0.2}FeO_3$	0.9350	0.6872	6.665	6.534	1.965
$Nd_{0.7}Sr_{0.3}FeO_3$	0.9408	0.3874	6.519	6.423	1.473
$Nd_{0.6}Sr_{0.4}FeO_3$	0.9467	0.2897	6.395	6.322	1.143
$Nd_{0.5}Sr_{0.5}FeO_3$	0.9526	0.2501	6.258	6.199	0.943

mass in grams, here deviation from stoichiometry is not taken into account while calculating *M*. *N* is the Avogadro's number and *V* is the volume in centimeter cube. The percentage porosity (*P*) in is calculated by using the following relation:

$$P = \left(\frac{1-d}{d_{th}}\right) \times 100 \quad (4)$$

In Table 2, the results of theoretical density (d_{th}), bulk density (*d*) and calculated percentage porosity (*P*) are given. From these results it is apparent that for all samples the bulk density is above 97% of the theoretical density and it further improves with increase in the strontium concentration. This can be attributed to the decrease in melting temperature with increase in the Sr concentration. Thus on the basis of reduction in the difference between *a* and *b* parameters, Goldsmith tolerance factor (*t*), percent orthorhombic distortion (*D*) and closeness of bulk density with theoretical density, it can be deduced that although system remained orthorhombic up to the 50% strontium concentration, however it moves toward more symmetric tetragonal/cubic structure.

In this study, fractured surfaces of the freshly synthesized pallets were examined; Fig. 3 shows the SEM micrographs of $Nd_{1-x}Sr_xFeO_3$ pellets sintered at 1300 °C. It is evident from these micrographs that grain sizes increase with increase in the strontium doping level; in addition, the grain connectivity has been improved. The increase in grain sizes may be due to lower melting point of the strontium oxide as compared to the melting point of neodymium oxide. Thus the higher strontium concentration samples have lower melting point as compared to un-doped $NdFeO_3$. Since, in this study all samples were sintered at the same temperature, therefore the samples containing higher dopant concentration have more grain growth and compaction than those having low concentration of strontium. From these results it is inferred that there is a gradual decrease in the porosity and an increase in the connectivity of the grains with increase in the strontium content. SEM analysis revealed that the grains are mostly well connected and intermixed. Some grains, especially in lower doped samples, have well defined geometrical shapes and sharp grain boundaries. With increase in the strontium content there is a gradual reduction in grain boundaries area, the grain

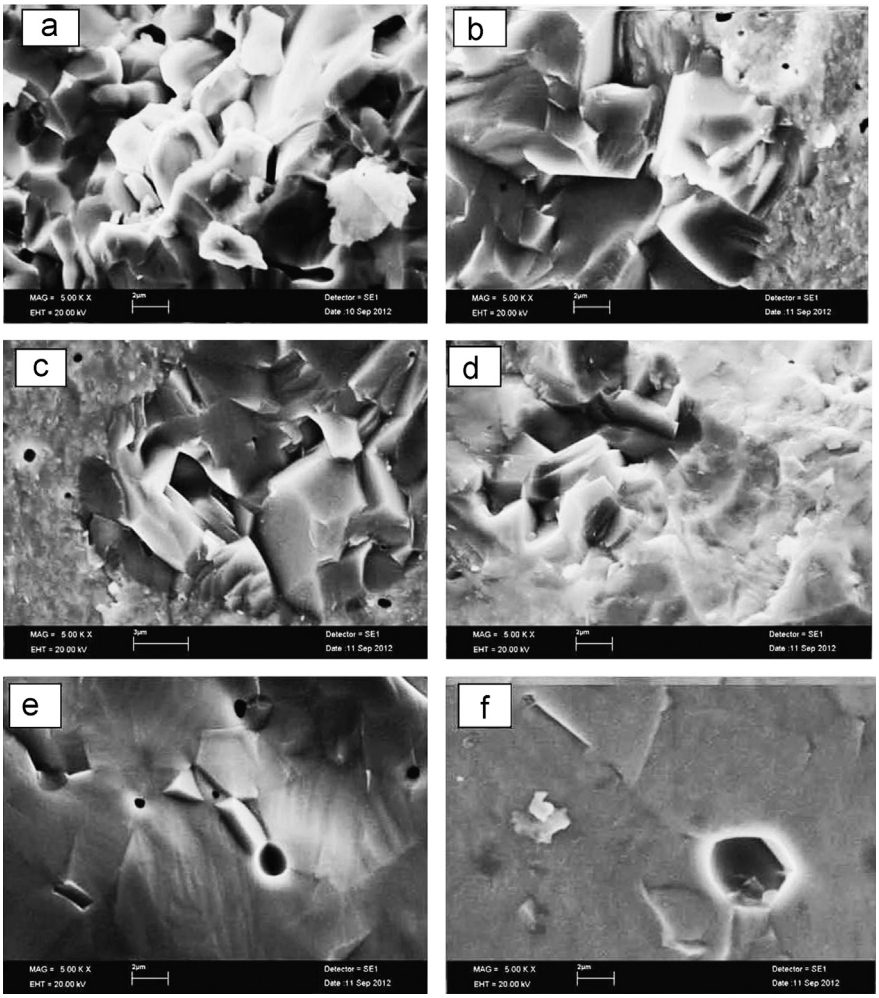

Fig. 3. SEM micrographs of (a) $NdFeO_3$ (b) $Nd_{0.9}Sr_{0.1}FeO_3$ (c) $Nd_{0.8}Sr_{0.2}FeO_3$ (d) $Nd_{0.7}Sr_{0.3}FeO_3$ (e) $Nd_{0.6}Sr_{0.4}FeO_3$ and (f) $Nd_{0.5}Sr_{0.5}FeO_3$ taken from the fractured surfaces of the sintered pellets.

boundaries are very well defined and sharp in $NdFeO_3$; however, higher Sr doped samples become more homogenous and intermixed. The observed pore size varies from area to area and sample to sample but mostly their size is less than 0.5 μm. The pores are produced due to the effects of sintering temperature, applied pressure to make pallets and pressing time while misorientation and mismatch of grains and grain boundaries can also play important role.

^{57}Fe Mössbauer spectroscopy is employed to investigate the effects of Sr doping on the local structure of $Nd_{1-x}Sr_xFeO_3$ system at room temperature. The Mössbauer spectra of $Nd_{1-x}Sr_xFeO_3$ samples are shown in Fig. 4 and fitted results of the analyses are given in Table 3. Fig. 4a shows room temperature Mössbauer spectrum of $NdFeO_3$, which is well fitted by a single sextet. The Mössbauer spectra of undoped orthoferrites, with 4f group cations at A-sites, below Neel temperature are well fitted by one Zeeman sextet indicating the magnetic ordering in the system and a singlet above Neel temperature [22]. The presence of a single sextet in $NdFeO_3$ indicates homogeneous phase formation, absence of magnetic impurity traces and identical environment of all Fe ions. The sharp peaks observed in Mössbauer spectrum are indicative of very less sagging in the system, single oxidation state of iron and phase purity. The values of hyperfine parameters provide clear evidence of typical Fe^{3+} high spin state in octahedral coordination [21,37–39]. The observed value of isomer shift is higher than the value of Fe^{4+} and lower than that of Fe^{2+}, demonstrating that almost all iron present in undoped $NdFeO_3$ have oxidation state of Fe^{3+}.

Fig. 4b shows the Mössbauer spectrum of $Nd_{0.9}Sr_{0.1}FeO_3$, which can be described by the presence of two sextets and a singlet. The magnetic hyperfine field of the first sextet is

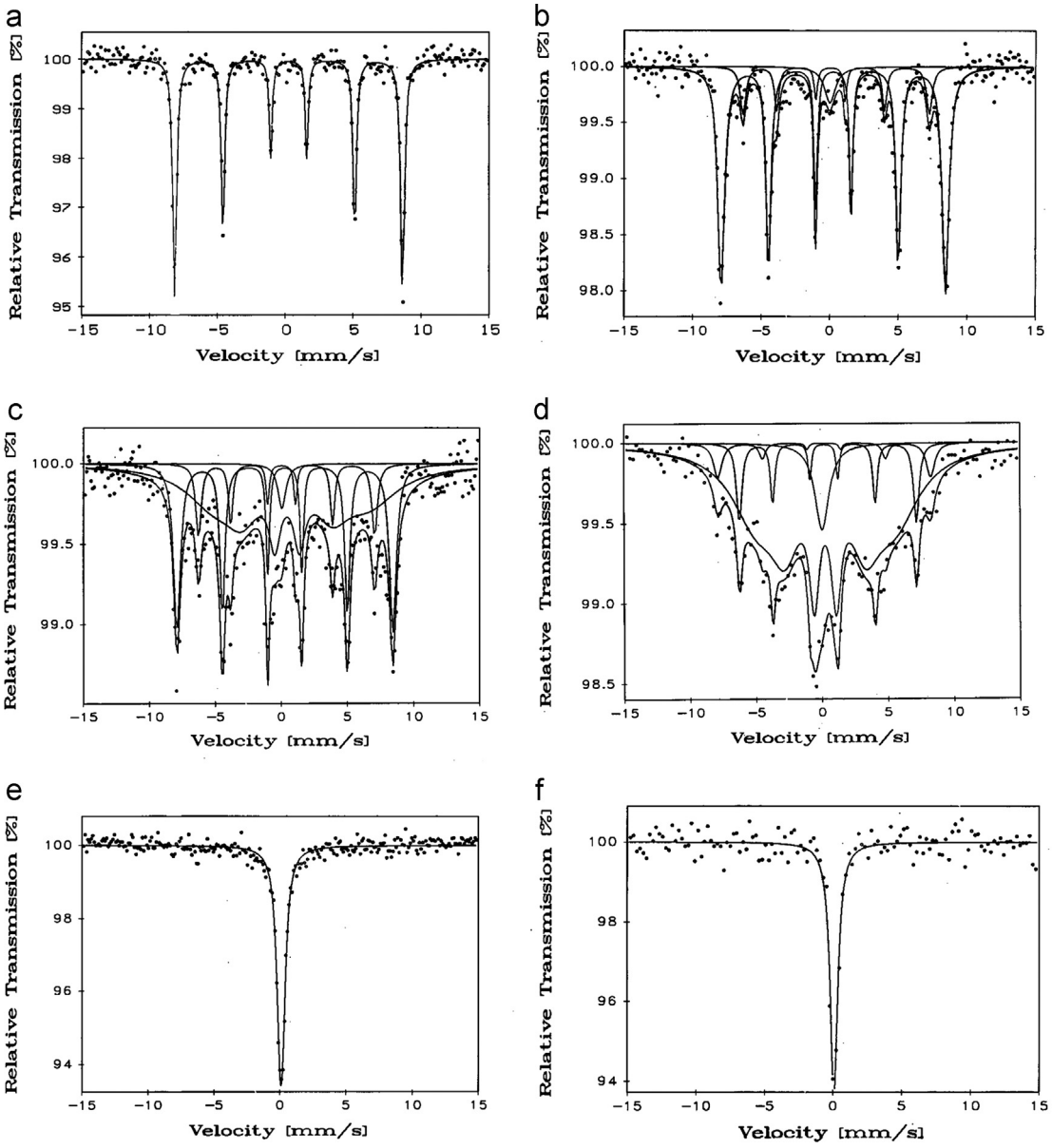

Fig. 4. Room temperature Mössbauer spectra of (a) $NdFeO_3$ (b) $Nd_{0.9}Sr_{0.1}FeO_3$ (c) $Nd_{0.8}Sr_{0.2}FeO_3$ (d) $Nd_{0.7}Sr_{0.3}FeO_3$ (e) $Nd_{0.6}Sr_{0.4}FeO_3$ and (f) $Nd_{0.5}Sr_{0.5}FeO_3$.

Table 3
Magnetic hyperfine field (H_B), isomer shift (IS), quadrupole splitting (Δ), line width (Γ) and relative area (%) associated with each spectral feature in ^{57}Fe Mossbauer spectra of $Nd_{1-x}Sr_xFeO_3$.

Sample		H_B (KOe)	IS (mm s^{-1})	Δ (mm s^{-1})	Γ (mm s^{-1})	Relative area (%)
$NdFeO_3$	Sextet	519	0.38	−0.028	0.34	100
$Nd_{0.9}Sr_{0.1}FeO_3$	Sextet A	507	0.37	−0.019	0.59	80
	Sextet B	421	0.36	0.39	0.50	15
	Singlet	–	0.12	–	0.99	5
$Nd_{0.8}Sr_{0.2}FeO_3$	Sextet A	507	0.37	−0.009	0.63	37
	Sextet B	414	0.32	0.36	0.50	11
	Sextet C	367	0.41	0.32	5.22	44
	Singlet	–	0.16	–	0.75	8
$Nd_{0.7}Sr_{0.3}FeO_3$	Sextet A	500	0.28	0.005	0.70	13
	Sextet B	416	0.41	0.28	0.50	9
	Sextet C	326	0.37	0.33	4.59	64
	Singlet	–	0.13	–	1.30	13
$Nd_{0.6}Sr_{0.4}FeO_3$	Singlet	–	0.19	0.22	0.65	100
$Nd_{0.5}Sr_{0.5}FeO_3$	Singlet	–	0.18	0.35	0.67	100

507 kOe and a second sextet appears with magnetic field of 421 kOe, having 15% relative area, showing decrease in magnetic ordering as compared to $NdFeO_3$. The values of magnetic field also indicate that Fe is in high spin state. The isomer shifts for these sextets are 0.37 and 0.36 indicating that Fe ions which are responsible for the formation of these sextets have +3 oxidation states. The observed 0.12 isomer shift value of singlet having approximately 5% relative area, corresponds to Fe^{4+} state. Kharton et. al. [25] have shown that for $Ln_{0.5}A_{0.5}FeO_3$ (where Ln=La, Pr, Nd, and Sm and A=Sr and Ba) the isomer shift range for Fe^{3+} is from 0.28–0.46 while isomer shift for Fe^{4+} is in the range of 0.09 and 0.14. Some other workers considered this observed isomer shift as intermediate value between Fe^{3+} and Fe^{4+}, which has two main origins. First is the presence of Fe cations with intermediate non-integer valence state between 3+ and 4+ owing to fast hole hoping between Fe^{3+} and Fe^{4+} at a time scale less than the Mössbauer experiment time window (10^{-8} s) [40–44]. Second explanation was given by Ryu et. al. [45] on the basis of small ionic radius and large positive charge on Fe^{4+} as compared to Fe^{3+} which causes an increase in the polarization of Fe–O bond. Consequently, negative charge of oxygen slightly shifts toward Fe^{4+} which causes a decrease in the charge on Fe and hence an intermediate value of isomer shift is observed. The observation of a singlet having isomer shift of 0.12 indicates the presence of iron with oxidation state higher than +3. The sextet A has zero quadrupole splitting value, suggesting that Fe environment is octahedral; while the quadrupole splitting value for sextet B is away from zero indicating that Fe is slightly shifted from its lattice site and its environment is not perfectly octahedral. The larger value of quadrupole splitting indicates an increase in the octahedral distortions, when compared with $NdFeO_3$. This increase in the octahedral distortion is opposite to the XRD results which showed an increase in the symmetry with increase in the Sr content; due to this opposing trend, the octahedral distortions are referred as anomalous. The possible reason for this behavior may be that Mössbauer spectroscopy, which is a microscopic technique, determines the minute changes in the local atomic and electronic structure around the probing nuclei via hyperfine interactions due to its high resolution. Whereas, XRD being a macroscopic technique cannot determine such tiny changes and only gives an average structure of a material. The increase in line width also indicates that distribution in hyperfine parameters is increased in $Nd_{0.9}Sr_{0.1}FeO_3$.

In Fig. 4c and d the Mössbauer spectra of $Nd_{0.8}Sr_{0.2}FeO_3$ and $Nd_{0.3}Sr_{0.3}FeO_3$ are shown; for these materials both spectra can be fitted well by three sextets and a singlet. This is mainly due to the formation of Fe^{4+}, change in the surrounding environment of Fe^{3+} and presence of steric effects, produced by bigger size of the strontium ion as compared to the neodymium ion. The values of hyperfine parameters of both spectra indicate that there is a gradual increase in the Fe^{4+} content, area of paramagnetic singlet and octahedral distortions while there is a decrease in the magnetic ordering with increase in the Sr concentration.

Room temperature Mössbauer spectra of $Nd_{0.6}Sr_{0.4}FeO_3$ and $Nd_{0.5}Sr_{0.5}FeO_3$ are shown in Fig. 4e and f. These spectra can be fitted by a singlet, where magnetic ordering is completely lost in both samples. The isomer shift values are intermediate between Fe^{3+} and Fe^{4+} which again indicate presence of Fe^{4+}, fast hole hopping between Fe^{3+} and Fe^{4+} and slight shift of oxygen negative charge toward Fe^{4+}. The quadrupole splitting values of both samples are away from zero indicating that octahedral distortions have increased with increase in the dopant concentration.

On the basis of Mössbauer study, we can confer the causes or origin behind the increase of octahedral distortions with increase in the Sr concentration in the $Nd_{1-x}Sr_xFeO_3$ system. From these results it has been observed that Fe^{4+}/Fe^{3+} ratio, which was approximately zero in $NdFeO_3$ has gradually increased with increase in the strontium concentration, may be responsible for these octahedral distortions. These local distortions around the Fe sites are not correlated to average A-site cations radii, lattice symmetry, unit cell volume and the tolerance factor. But, these are more associated with the concentration and sizes of Fe^{4+} and Fe^{3+} ions, bond lengths of Fe^{4+}–O^{-2} and Fe^{3+}–O^{-2}, mismatch between ionic radii of A-site cations, decrease in the oxidation state of A-site cation (due to the replacement of Nd^{3+} by Sr^{2+}) and also it may be due to slight change in oxygen stoichiometry. The effects of oxidizing and reducing environments on the Fe oxidation state, oxygen

stiochoimetry and Neel temperature were investigated by Brinks et. al. [24] for $Pr_{1-x}Sr_xFeO_3$; it was shown that the oxygen stoichiometry vary significantly in reducing environment, however in oxidized environment oxygen stoichiometry did not differ considerably. In the present study, samples were synthesized in oxidized environment, therefore it is anticipated that there is not any appreciable variation in the oxygen stoichiometry. The increase in concentration of Fe^{4+}, decrease in oxidation state of A-site cations and mismatch between ionic radii of Nd^{3+} and Sr^{2+} may have pronounced effects on the surrounding environment. Hence, these factors can be attributed to the origin of increase in octahedral distortions in the $Nd_{1-x}Sr_xFeO_3$ system with increase in the strontium content.

As evident from the Mössbauer spectra of $Nd_{1-x}Sr_xFeO_3$ samples, possible causes for the collapse of magnetically ordered state to spin disordered state are: the high spin to low spin transition of Fe, increase in the spin–spin relaxation frequency and decrease in strength for the super-exchange interactions with increase in the strontium concentration. Makhdoomi et.al. [39] have suggested that as the octahedral distortions around Fe increase, the crystal field splitting energy increases and exceeds the average electron spin pairing energy; consequently spin configuration of the Fe^{3+} ion crosses over from a high spin to a low spin state. This was ascertained by the progressive decrease of the associated internal hyperfine field and increase in sagging of the magnetic sextet. The observed decrease in the value of associated isomer shift was attributed to the decrease in the cell volume, which caused an increase in the s-electron density around Fe nuclei. Although, the observed values of the associated internal hyperfine field in the present study (as given in Table 3) decrease with increase in the Sr concentration; however, it cannot be correlated to a low spin Fe^{3+} with only one unpaired spin. The magnetic field associated with the sextet A, B and C present in $Nd_{0.7}Sr_{0.3}FeO_3$ is 500 kOe, 416 kOe and 326 kOe, respectively. These values are higher than the magnetic field allied with the low spin Fe^{3+} (H_{LS}) which should be around or below 100 kOe, because of the relation ($5/2:1/2::H_{HS}:H_{LS}$). Therefore, the possibility of iron being in low spin state Fe^{3+} ion can be ruled out particularly up to 30% strontium concentration. However, high spin Fe^{4+} have four unpaired spins which are relatively lower than five unpaired spins of Fe^{3+} which can play important role.

Another explanation for the sagging behavior and lowering of the Neel temperature was given by Marzec [46], where temperature and composition dependant sagging of the sextets in orthoferrites was elucidated. In that study the justification for the transition from a magnetically ordered state to a spin disordered state by the spin–spin relaxation frequency phenomena was presented, which become faster than the characteristic Mössbauer experiment time window. Increase in the spin–spin relaxation frequency with temperature and composition can account for the sagging of the sextet and collapse of the magnetically ordered state in orthoferrite systems. Kharton et. al. [25] have investigated $Nd_{0.5}Sr_{0.5}FeO_3$ by using Mössbauer spectroscopy at 4.1 K and 297 K. At 4.1 K magnetic field was 515 kOe, while at 297 K the magnetic ordering was completely lost; which shows that this material has Neel temperature below room temperature. In the present study, on the basis of magnetic ordering results, it can be inferred that up to 30% strontium doping $Nd_{1-x}Sr_xFeO_3$ system may have Neel temperature above room temperature; whereas when the Sr concentration is higher than 40%, the Neel temperature shifts below room temperature.

Strength of the super-exchange interactions depends upon the nature of the B site cations and angle of B–O–B path; as the Sr concentration increases, it causes an increase in the Fe^{4+} content. Thus the observed decrease in the magnetic ordering can also be correlated to the increase in Fe^{4+} content, which results in a weaker Fe^{3+}–O^{-2}–Fe^{4+} double exchange interactions as compared to Fe^{3+}–O^{-2}–Fe^{3+} superexchange interactions and change in the Fe–O–Fe bond angle due to increase in the concentration of strontium. Brinks et. al. [24] have investigated $Pr_{1-x}Sr_xFeO_3$ synthesized both in reducing and oxidizing environments. For samples synthesized in reducing environment they found that all Fe ions have 3+ oxidation state and as a result of Fe^{3+}–O^{-2}–Fe^{3+} super-exchange interactions, a very small change in the Neel temperature (T_N=711 K for x=0 and 700 K for x=0.67) was detected. However, for samples prepared in oxidized environment due to presence of Fe^{3+}–O^{-2}–Fe^{4+} double exchange interactions, the Neel temperature decreased significantly (T_N=711 K for x=0 and 190 K for x=0.50); moreover, the collapse of magnetic ordering was also observed in the oxidized samples at room temperature. Hence, based on the above discussion it can be summarized that weakening of the super-exchange interactions, increase in the spin–spin relaxation frequency and dilution of the strong long range magnetic sub-lattices of high spin Fe^{3+} (five unpaired spins) by relatively lower spin (four unpaired spins) of high spin Fe^{4+}, are the major factors responsible for the collapse of magnetic ordering in the $Nd_{1-x}Sr_xFeO_3$ orthoferrite system.

4. Conclusion

In the present study the single phase polycrystalline $Nd_{1-x}Sr_xFeO_3$ system, (where x=0–0.5), has been synthesized by the solid state reaction method. XRD results verified phase purity, increase in the symmetry and tolerance factor while decrease in the orthorhombic distortion and density with increase in the strontium concentration. Comparison of pycnometer bulk density with XRD theoretical density indicated a decrease in the porosity with increase in the strontium content. SEM analyses illustrated an increase in the grain size and a decrease in the porosity. Mössbauer spectroscopy results indicated an increase in the Fe^{4+}/Fe^{3+} ratio, sagging and local octahedral distortions while decrease in the magnetic ordering with increase in the strontium concentration. The origin of anomalous octahedral distortions present in the $Nd_{1-x}Sr_xFeO_3$ system can be attributed to the increase in the concentration of Fe^{4+}, mismatch between the ionic radii and decrease in the oxidation state of A-site cations (due to the substitution of Sr^{2+} at Nd^{3+} sites). However, the major factors behind the collapse

of magnetic ordering in this orthoferrite system may be weakening of the super-exchange interactions, increase in the spin–spin relaxation frequency and dilution of the strong long range magnetic sub-lattices of high spin Fe^{3+} (five unpaired spins) by relatively lower spin (four unpaired spins) of high spin Fe^{4+}.

Acknowledgments

One of the authors, Irfan Ahmad thanks the Higher Education Commission (HEC) of Pakistan for the financial support through 5000 Indigenous Scholarship Scheme in Physical Sciences Batch-V for his Ph.D. studies. The authors are grateful to MRG, Materials Division, PINSTECH for providing XRD facility. Authors also acknowledge PAEC for supporting this project.

References

[1] M.J. Akhter, C.R.A. Catlow, B. Slater, A.M. Walker, S.M. Woodley, Bulk and surface simulation studies of $La_{1-x}Ca_xMnO_3$, Chemistry of Materials 18 (2006) 1552–1560.
[2] R.T.A. Khan, M.J. Akhter, Atomistic computer simulation studies of $La_{1-x}Sr_xVO_3$, Solid State Communication 137 (2006) 110–114.
[3] J. Zaanen, G.A. Sawatzaky, J.W. Allen, Band gaps and electronic structure of transition-metal compounds, Physical Review Letters 55 (1985) 418–421.
[4] J.G. Bendnorz, K.A. Müller, Possible high T_c superconductivity in the Ba–La–Cu–O system,, Physica B: condensed Matter 64 (1986) 189–193.
[5] G. Binning, A. Baratoff, H.E. Honig, J.G. Bednorz, Two-band superconductivity in Nb-doped $SrTiO_3$, Physical Review Letters 45 (1980) 1352–1355.
[6] M. Imada, A. Fujimori, Y. Tokura, Metal-insulator transitions, Physical Review Letters 70 (1998) 1039–1263.
[7] K. Sreedhar, J.M. Honig, M. Darwin, M. McElfresh, P.M. Shand, J. Xu, B.C. Crooker, J. Spalek, Electronic properties of the metallic perovskite $LaNiO_3$: Correlated behavior of 3*d* electrons, Physical Review B 46 (1992) 6382–6386.
[8] R.V. Helmolt, J. Wecker, B. Holzapfel, L. Schultz, K. Samwer, Giant negative magnetoresistance in perovskitelike $La_{2/3}Ba_{1/3}MnO_x$ ferromagnetic films, Physical Review Letters 71 (1993) 2331–2333.
[9] K. Chahara, T. Ohno, M. Kasai, Y. Kozono, Magnetoresistance in magnetic manganese oxide with intrinsic antiferromagnetic spin structure, Applied Physics Letters 63 (1993) 1990–1992.
[10] C.Y. Park, F.V. Azzarello, A.J. Jacobson, The oxygen non-stoichiometry and electrical conductivity of $La_{0.7}Sr_{0.3}Cu_{0.2}Fe_{0.8}O_{3-\delta}$, Journal of Material Chemistry 16 (2006) 3624–3628.
[11] N.Q. Minh, Ceramic fuel cells, Journal of the American Ceramic Society 76 (1993) 563–588.
[12] H. Ullmann, N. Trofimenko, F. Tietz, D. Stöver, A. Ahmad-Khanlou, Correlation between thermal expansion and oxide ion transport in mixed conducting perovskite-type oxides for SOFC cathodes, Solid State Ionics 138 (2000) 79–90.
[13] J. Choi, J.H. Lee, D.S. Park, B.D. Hahn, W.H. Yoon, H. Lin, Oxidation resistance coating of LSM and LSCF on SOFC metallic interconnects by the aerosol deposition process, Journal of the American Ceramic Society 90 (2007) 1926–1929.
[14] M.J. Akhtar, Z.N. Akhtar, J.P. Dragun, C.R.A. Catlow, Electrical conductivity and extended X-ray absorption fine structure studies of $SrFe_{1-x}Nb_xO_3$ and $BaFe_{1-x}Nb_xO_3$ systems, Solid State Ionics 104 (1997) 147–158.
[15] H.J.M. Bouwmeester, H. Kruidhof, A.J. Burggraf, Importance of the surface exchange kinetics as rate limiting step in oxygen permeation through mixed-conducting oxides, Solid State Ionics 72 (1994) 185–194.
[16] Y.S. Didosyan, H. Hauser, V.Y. Barash, P.L. Fulmek, Subsonic domain wall dynamics in yttrium orthoferrite, Journal of Magnetism and Magnetic Materials 177 (1998) 203–204.
[17] G. Martinelli, M. Carotta, M. Ferroni, E. Traversa, Screen-printed perovskite-type thick films as gas sensors for environmental monitoring, Sensors and Actuators B 55 (1999) 99–110.
[18] M.V. Chetkin, Y.N. Kurbatova, T.B. Shapaeva, Gyroscopic dynamics of antiferromagnetic vortices in the orthoferrite domain wall, Journal of Magnetism and Magnetic Materials 321 (2009) 800–802.
[19] N. Dasgupta, R. Krishnamoorthy, K.T. Jacob, Crystal structure and thermal and electrical properties of the perovskite solid solution $Nd_{1-x}Sr_xFeO_{3-\delta}$($0 \le x \le 0.4$), Solid State Ionics 149 (2002) 227–236.
[20] A. Bashir, M. Ikram, R. Kumar, P. Thankur, K.H. Chae, Structural, magnetic and electronic structure studies of $NdFe_{1-x}Ni_xO_3$ ($0 \le x \le 0.3$), Journal of Physics: Condensed Matter 21 (2009) 325501.
[21] I. Ahmad, M.J. Akhtar, M. Younas, M. Siddique, M.M. Hasan, Small polaronic hole hopping mechanism and Maxwell–Wagner relaxation in $NdFeO_3$, Journal of Applied Physics 112 (2012) 074105.
[22] M. Eibschutz, S. Shtrikman, D. Treves, Mössbauer studies of Fe^{57} in orthoferrites, Physical Reviews 156 (1967) 562–577.
[23] A. Tiwari, Local environment of Fe in $NdFe_{1-x}Ni_xO_{3-\delta}$ perovskite oxides, Journal of Alloys and Compounds 274 (1998) 42–46.
[24] H.W. Brinks, H. Fjellvag, A. Kjekshus, B.C. Hauback, Structure and magnetism of $Pr_{1-x}Sr_xFeO_{3-\delta}$, Journal of Solid State Chemistry 150 (2000) 233–249.
[25] V.V. Kharton, A.V. Kovalevsky, M.V. Patrakeev, E.V. Tsipis, A.P. Viskup, V.A. Kolotygin, A.A. Yaremchenko, A.L. Shaula, E.A. Kiselev, J.C. Waerenborgh, Oxygen nonstoichiometry, mixed conductivity, and Mössbauer spectra of $Ln_{0.5}A_{0.5}FeO_{3-\delta}$(Ln = La–Sm, A = Sr, Ba): effects of cation size, Chemistry of Materials 20 (2008) 6457–6467.
[26] A.A. Chainani, M. Mathew, D.D. Sharma, Electronic structure of $La_{1-x}Sr_xFeO_3$, Physical Review B 48 (1993) 14818–14825.
[27] M. Viviani, M. Bassoli, V. Buscaglia, M.T. Buscaglia, P. Nanni, Giant permittivity and Maxwell–Wagner relaxation in Yb:$CaTiO_3$ ceramics, Journal of Physics D: Applied Physics 42 (2009) 175407.
[28] M. Li, A. Feteira, D.C. Sinclair, Origin of the high permittivity in $(La_{0.4}Ba_{0.4}Ca_{0.2})(Mn_{0.4}Ti_{0.6})O_3$ ceramics, Journal of Applied Physics 98 (2005) 084101.
[29] E. Kuzmann, S. Nagy, A. Vertes, Critical review of analytical applications of Mössbauer spectroscopy illustrated by mineralogical and geological examples, Pure and Applied Chemistry 75 (2003) 801–858.
[30] M.I. Oshtrakh, Biomedical applications of Mössbauer spectroscopy, Journal of Radioanalytical and Nuclear Chemistry 269 (2006) 407–415.
[31] T.C. Gibbs, Principles of Mössbauer Spectroscopy, Chapman and Hall, London, 1976.
[32] H. Frauenfelder, W.A. Banjamin, The Mössbauer Effect, W.A. Benjamin, Inc., New York, 1962.
[33] J. Blasco, J. Garcia, Structural, magnetic and electrical properties of $NdNi_{1-x}Fe_xO_3$ and $NdNi_{1-x}Co_xO_3$ systems, Journal of Physics and Chemistry of Solids 55 (1994) 843–852.
[34] W. Slawinski, R. Przenioslo, I. Sosnowska, E. Surad, Spin reorientation and structural changes in $NdFeO_3$, Journal of Physics: Condensed Matter 17 (2005) 4605.
[35] R.D. Shannon, Revised effective ionic radii and systematic studies of interatomic distances in halides and chalcogenides, Acta Crystallography A 32 (1976) 751.
[36] G.C. Kostogloudis, N. Vasilakos, C. Ftikos, Preparation and characterization of $Pr_{1-x}Sr_xMnO_{3\pm\delta}$ ($x=0$, 0.15, 0.3, 0.4, 0.5) as a potential SOFC cathode material operating at intermediate temperatures (500–700 °C), Journal of the European Ceramic Society **17** (1997) 1513–1521.
[37] A.A. Leontiou, A.K. Ladavos, T.V. Bakas, T.C. Vaimakis, P. Pomonis, Reverse uptake of oxygen from $La_{1-x}Sr_x(Fe^{3+}/Fe^{4+})O_{3\pm\delta}$ perovskite-type mixed oxides ($x=0.00$, 0.15, 0.30, 0.40, 0.60, 0.70, 0.80, 0.90), Journal of Applied Catalysis A: General 241 (2003) 143–154.
[38] A. Delmastro, D. Mazza, S. Ronchetti, M. Vallino, R. Spinicci, P. Brovetto, Synthesis and characterization of non-stoichiometric

$LaFeO_3$ perovskite, Materials Science and Engineering B 79 (2001) 140–145.

[39] A.B. Makhdoomi, M. Ikram, R. Kumar, Mössbauer studies and magnetic studies of Ni doped orthoferrites $PrFe_{1-x}Ni_xO_3$ ($x \leq 0.3$), Journal of Magnetism and Magnetic Materials 322 (2010) 2581–2584.

[40] M. Danot, M.I. Afanasov, P.B. Fabritchnyi, A.S. Golub, N.D. Lenenko, Y.N. Novikov, K.V. Pokholok, I.A. Presniakov, Mössbauer evidence for fast electron hopping between Fe(II) and Fe(III) in iron hydroxide/molybdenum disulfide lamellar nanocomposite, Solid State Ionics 128 (2000) 211–216.

[41] K.V. Pokholok, D.S. Fillimonov, N.A. Pichugin, A.P. Malakho, V. P. Gorkov, N.N. Savvateev, Effect of oxygen vacancy disordering on electronic processes in perovskite-like $SrFe_{1-x}Sc_xO_{3-\gamma}$ ferrites, Russian Journal of Inorganic Chemistry 50 (2005) 267–273.

[42] Y. Rizki, J.M.L. Breton, E. Floke, L. Lechevallier, Y. Bread, A. Maigman, A Mössbauer spectroscopy investigation of $SrFe_{1-x}Sc_xO_{3-\delta}$ perovskites, Solid State Science 12 (2010) 739–744.

[43] M. Takano, J. Kawachi, N. Nakanishi, Y. Takeda, Valence state of the Fe ions in $Sr_{1-y}La_yFeO_3$, Journal of Solid State Chemistry 39 (1981) 75–84.

[44] P.D. Battle, T.C. Gibb, S. Nixon, A study of charge disproportionation in the nonstoichiometric perovskite $Sr_2LaFe_3O_{8+y}$ by Mössbauer spectroscopy, Journal of Solid State Chemistry 77 (1988) 124–131.

[45] K.S. Ryu, S.J. Lee, C.H. Yo, Study of nonstoichiometry and physical properties of the perovskite $Sr_xHo_{1-x}FeO_{3-y}$ system, Bulletin of the Korean Chemical Society 15 (1994) 256–260.

[46] J. Marzec, Hyperfine interactions in $LaFe_{1-x}Ni_xO_{3-d}$, $La_{0.4}Sr_{0.6}Co_{0.2}Fe_{0.8}O_{3-d}$ and $La_{1-x}Sr_xCo_{1-y-z}Fe_yNi_zO_{3-d}$ perovskites, Journal of Power Sources 173 (2007) 671–674.